ELSEVIER

Marine Geology 247 (2008) 46–60

MARINE GEOLOGY
INTERNATIONAL JOURNAL OF MARINE GEOLOGY, GEOCHEMISTRY AND GEOPHYSICS

www.elsevier.com/locate/margeo

Scale invariant characteristics of the Storegga Slide and implications for large-scale submarine mass movements

Aaron Micallef *,[1], Christian Berndt, Douglas G. Masson, Dorrik A.V. Stow

National Oceanography Centre, University of Southampton, European Way, Southampton, SO14 3ZH, UK

Received 19 April 2007; received in revised form 9 August 2007; accepted 23 August 2007

Abstract

This study documents the fractal characteristics of submarine mass movement statistics and morphology within the Storegga Slide. Geomorphometric mapping is used to identify one hundred and fifteen mass movements from within the Storegga Slide scar and to extract morphological information about their headwalls. Analyses of this morphological information reveal the occurrence of spatial scale invariance within the Storegga Slide. Non-cumulative frequency-area distribution of mass movements within the Storegga Slide satisfies an inverse power law with an exponent of 1.52. The headwalls exhibit geometric similarity at a wide range of scales and the lengths of headwalls scale with mass movement areas. Composite headwalls are self-similar.

One of the explanations of the observed spatial scale invariance is that the Storegga Slide is a geomorphological system that may exhibit self-organized criticality. In such a system, the input of sediment is in the form of hemipelagic sedimentation and glacial sediment deposition, and the output is represented by mass movements that are spatially scale invariant. In comparison to subaerial mass movements, the aggregate behavior of the Storegga Slide mass movements is more comparable to that of the theoretical 'sandpile' model. The origin of spatial scale invariance may also be linked to the retrogressive nature of the Storegga Slide. The geometric similarity in headwall morphology implies that the slope failure processes are active on a range of scales, and that modeling of slope failures and geohazard assessment can extrapolate the properties of small landslides to those of larger landslides, within the limits of power law behavior. The results also have implications for the morphological classification of submarine mass movements, because headwall shape can be used as a proxy for the type of mass movement, which can otherwise only be detected with very high resolution acoustic data that are not commonly available.

Keywords: Storegga Slide; scale invariance; power law; self-organized criticality; 'sandpile' model; retrogressive cascade

1. Introduction

Submarine landslides are common phenomena on continental margins. Large landslides are the dominant geomorphic agents that transfer sediment across the continental slope (Masson et al., 2006), and they play a major role in the evolution of submarine landscapes. The Storegga Slide, located 120 km offshore Norway, is the largest known submarine landslide (Fig. 1). Dated at 8100±250 cal yrs BP (Haflidason et al., 2005), the Storegga Slide is the last in a series of slope failures that have characterized the mid-Norwegian Margin during the past 2.6 Ma (Solheim et al., 2005). The Storegga

* Corresponding author. Tel.: +44 23 80 596563; fax: +44 2380 596554.
E-mail address: amicall@noc.soton.ac.uk (A. Micallef).
[1] Present address: 16, Triq l-Ghakkies, Naxxar, NXR 05, Malta.

0025-3227/$ - see front matter © 2007 Elsevier B.V. All rights reserved.
doi:10.1016/j.margeo.2007.08.003

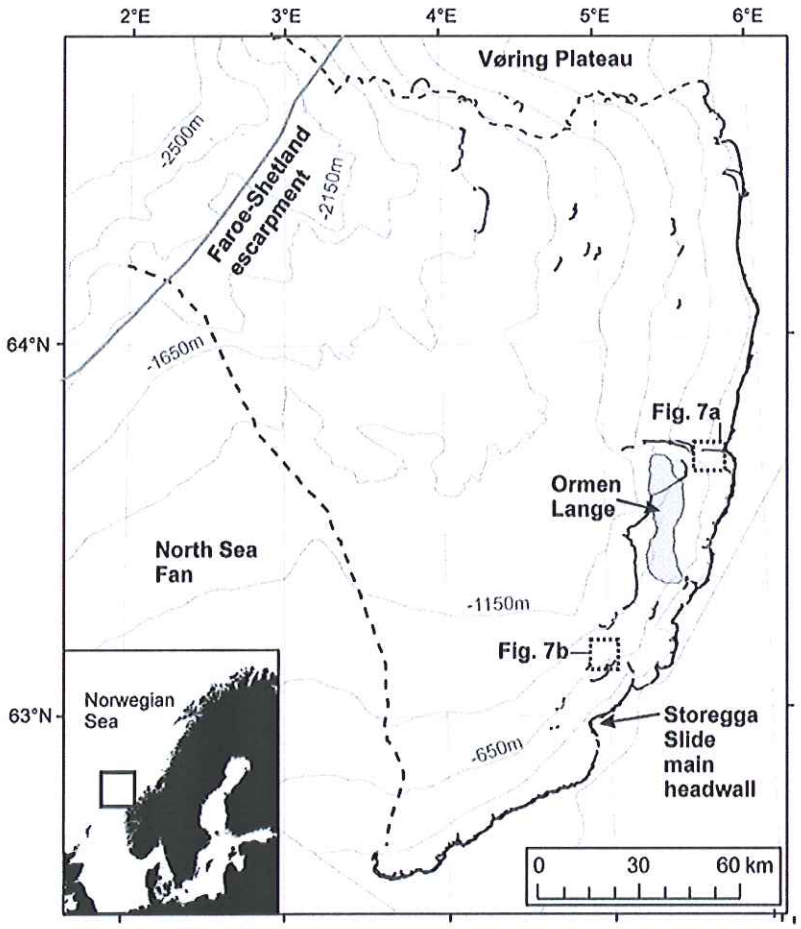

Fig. 1. Bathymetric map of the Storegga Slide. Bathymetric contours at 250 m intervals are shown as grey lines, whereas the extracted headwalls are represented by solid black lines. The dashed black line indicates the boundaries of the Storegga Slide. The location of the slide is shown in the inset.

Slide consisted of sixty-three quasi-simultaneous mass movements, which span an area of 95 000 km^2 and have evacuated 2400–3200 km^3 of sediment (Haflidason et al., 2004). These mass movements formed an amphitheatrical depression that contains numerous headwalls and scarps, the largest of which being the 320 km long main headwall located at the shelf break. The scar also encloses morphological features recognized as spreads, debris flows, turbidity flow channels and compressional ridges, which occur across a depth range of ~2700 m. The sedimentological framework of the Storegga Slide area is characterized by the alternation of glacial diamictons and ice-proximal sediments, deposited during glacial maxima, and fine-grained glacimarine, hemipelagic and contouritic sediments, deposited during interglacials (Berg et al., 2005). Because of its complexity and size, we consider the Storegga Slide as a macro-scale geomorphological system (10^2–10^6 km^2 in area, according to Summerfield (1991)).

Concepts associated with non-linear dynamic systems, such as fractals, chaos and self-organization, have gained considerable attention in many aspects of the geosciences. The fractal model, for instance, captures aspects of topography that other morphometric measures do not (Klinkenberg, 1992), and it provides a powerful approach to the representation of geoscientific data. The growing use of digital elevation models and the increasing resolution of topographic data sets have enabled geomorphologists to identify fractal structures and scale invariance in numerous subaerial environments (e.g. Pelletier, 1999; Southgate and Möller, 2000). The statistical characteristics of large populations of landslides, for example, have become a recent focus of study in geology and geomorphology (e.g. Guzzetti et al., 2002; Hergarten, 2003; Turcotte et al., 2006). Submarine mass movements, however, are still generally studied as isolated slope failure events using an engineering approach (e.g. Kvalstad et al., 2005; Sultan

et al., 2004). As the exploration and exploitation of the ocean floor move into the deeper continental slope, there is an increasing demand for the quantification of risk associated with submarine slope failures. Probabilistic hazard assessments, for example, depend on the extrapolation of mass movement inventories. In order to perform such assessments, the frequency–magnitude relations of mass movements and their scaling behavior must be identified and understood (Wolman and Miller, 1960).

The available statistics of submarine mass movement data are generally poorly characterized when compared to those of subaerial mass movements. The Storegga Slide scar, on the other hand, has been thoroughly surveyed using state-of-the-art acoustic imaging techniques. This provides us with the opportunity to investigate this geomorphological system at a large-scale and carry out a statistical and fractal analysis of the constituent mass movements. The purpose of the study is to: (a) Assess whether the Storegga Slide exhibits scale invariance in terms of the statistics and morphology of its constituent mass movements; (b) Identify the origin of the scale invariance in terms of system dynamics and geological processes, and understand its implications.

2. Conceptual framework

A fractal is a term coined to define a set/function for which the Hausdorff–Besicovitch dimension exceeds the topological dimension (Mandelbrot, 1977). Fractal geometry includes shapes characterized by irregularities that conform to non-Euclidean structures. The best way to describe a fractal is through its attributes. The most important characteristic of a fractal geometric object is self-similarity at a variety of scales, whereby the object contains scaled copies of itself. Another attributes of a fractal object are infinite length and complexity. Known as the Steinhaus paradox (Steinhaus, 1960), the degree of detail of a fractal object increases infinitely as the scale decreases. A fundamental property of fractal objects is their fractal or similarity dimension (D). This is a single, non-integer value representing the scaling relationship between the apparent length and measuring scale. The fractal dimension also gives a useful measure of the complexity or roughness of a spatial pattern. The fractal dimension of linear features, for example, can vary between 1 for a straight line, and 2 for a feature so irregular that it fills an entire two-dimensional space (Mandelbrot, 1983). Unlike mathematical fractals, natural objects are not strictly self-similar, but rather statistically self-similar. In a statistically self-similar object, measurable statistical parameters are repeated at all scales. The object does not comprise exact copies of itself at all scales, but the object will contain no geometric indication of its scale (Goodchild and Mark, 1987).

The self-similar properties of data inventories, on the other hand, are investigated using frequency–magnitude relationships. A power law distribution implies that when we compare the number of events of size A or greater, with the number of events of size ηA or greater (where η is an arbitrary factor), the number always differs by the same factor of $\eta^{-\beta}$, regardless of the absolute size of the events. It has also been shown that the power law distribution can be replaced with other measures of the size of the event (Hergarten, 2003). This means that a power law distribution is free of a characteristic scale and is thus fractal (Mandelbrot, 1983).

3. Materials and methods

3.1. Data sets

Our investigation of the Storegga Slide is mainly based on a high resolution multibeam bathymetry data set that covers the slide scar from the main headwall down to a water depth of ca. 2700 m (Fig. 1). The grid generated from these multibeam data has a horizontal resolution of 25 m or better. Two other acoustic data sets complement our analyses. The first comprises Towed-Ocean-Bottom-Instrument (TOBI) sidescan sonar imagery that covers 20 000 km^2 of the slide area with a nominal horizontal resolution of 6 m. The second consists of high resolution 2D seismic lines, located across the main headwall and northern sidewall, and 2000 km^2 of industry-type 3D seismic data located across the northern sidewall.

3.2. Extraction of headwalls and estimation of the area of mass movements

We define a mass movement as a single episode of slope failure where sediment moves downslope under the influence of gravity. Spreads and debris flows are the most common mass movements within the Storegga Slide (Micallef et al., 2007). We define a spread as the extensional downslope displacement of a surficial mass of sediment on gently sloping ground, and a debris flow as moving laminar flows of agglomerated particles held together by a cohesive sediment matrix. The deposits associated with these mass movements are characterized by either a repetitive pattern of parallel ridges and

troughs (for spreads, Micallef et al. (2007)) or a blocky texture (for debris flows).

Mass movement area is a suitable proxy for the magnitude of mass movement events (Guzzetti et al., 2005). Area, volume and thickness of mass movements were shown to be strongly correlated with each other, and a distribution can be converted between these variables (e.g. Hergarten, 2003; Hovius et al., 1997; Pelletier et al., 1997). Measurements of area tend to be more reliable than those of volume or energy (Canals et al., 2004). The delineation of the boundaries of mass movements in a complex retrogressive landslide like the Storegga Slide is, however, difficult. This is because the distal parts of some mass movements have collapsed over a headwall and evolved into different types of mass movements (Micallef et al., 2007). The mass movements within the Storegga Slide occurred quasi-simultaneously (Haflidason et al., 2005), and the deposits of some mass movements have intersected or overlapped other deposits. TOBI sidescan sonar imagery is not available for the entire slide scar, which makes the differentiation between seafloor textures and the boundaries of adjacent mass movements more problematic. All of these factors lead to a degree of inaccuracy when estimating the areas of submarine mass movements within the Storegga Slide. In comparison to mass movement boundaries, headwalls constitute prominent morphological features that are both easily identifiable and large compared to noise in the data. The terminations of a headwall are defined by the zone where sediment movement has occurred perpendicularly to the headwall (in contrast to parallel, which defines the sidewall).

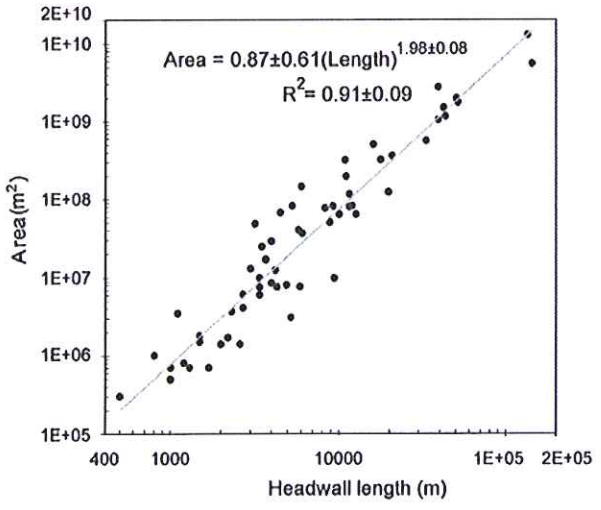

Fig. 2. Plot of headwall length vs. mass movement area of the fifty-eight individual slide events identified in Haflidason et al. (2004).

Previous studies, based on the visual interpretation of bathymetric and sidescan sonar data from the Storegga Slide, have identified sixty-three mass movements and determined their dimensions (Haflidason et al., 2004). We first used these published data to investigate the relationship between headwall length and mass movement area within the Storegga Slide (Fig. 2). We excluded the five larger lobes (lobes 1–5 in Haflidason et al. (2004)) from this relationship because their boundaries have not been constrained accurately and because each lobe comprises numerous mass movements. $R^2 = 0.91 \pm 0.09$ implies a strong statistical dependency between area and length in the form of a power law:

$$A = 0.87 \pm 0.61\, l^{1.98 \pm 0.08} \quad (1)$$

where

A area of mass movement (in m^2)
l length of headwall (in m)

We assume that this relationship applies to all mass movements within the Storegga Slide, and that we are able to estimate the area of a mass movement if we know the length of the associated headwall.

Building on this simple analysis, the headwalls of the mass movements were extracted automatically from the bathymetric data set. A geomorphometric map, which is a parametric representation of a landscape decomposed into its elementary morphological units, was generated for the study area. The morphological units, which include breaks and changes of slope, are extracted automatically as lineaments that are complemented by topographic information. The method of producing a geomorphometric map is described in Micallef et al. (2007). Headwalls, identified as continuous lineaments of breaks of slope, were assigned to a mass movement by using the sidescan sonar imagery, seismic data and geological information available in the literature. The types of mass movement were interpreted on the basis of morphology or internal structure. The terminations of the headwalls were determined manually by identifying the sections of the breaks of slope where sediment has been mobilized in a direction perpendicular to the lineaments. The lineaments that comprise a headwall were then grouped together and reduced into a single lineament having a thickness of one cell.

Using geomorphometric mapping we were able to identify one hundred and fifteen headwalls, which include the headwalls of the fifty-eight individual mass movements identified by Haflidason et al. (2004) and fifty-seven newly discovered mass movements. The headwalls of the

latter comprised forty-seven escarpments created by single (termed individual headwalls) and ten multiple (termed composite headwalls) mass movement events (Fig. 1; see also supplementary material). The co-ordinates of each vertex point in all of the one hundred and fifteen headwall lineaments were extracted, and the length of each headwall was calculated from these. The area associated with each headwall of the forty-seven newly discovered individual mass movements was estimated using Eq. (1). A cumulative frequency-area graph was plotted for all the one hundred and five individual mass movements, from which a non-cumulative distribution was derived.

3.3. Determining the fractal dimension D of headwalls

Numerous methods have been proposed to determine the fractal dimension of topography (Klinkenberg and Goodchild, 1992; Mandelbrot, 1983). Only a few of these are suitable for calculating the fractal dimension of 2D features (Klinkenberg, 1994). We used a standard technique known as the divider method. The basis for this vector-based technique is that the statistical variation between samples is a function of the distance between them. A divider is "walked" along the headwall lineament using a set width step (τ) and the number of steps required to cover the entire line is recorded. This number is then used to calculate the length of the lineament (L). τ is then increased by a fixed increment and the stepping process is repeated. The relation between length of the steps and calculated length of the lineament is:

$$L \propto \tau^{1-D} \tag{2}$$

The fractal dimension D can thus be determined by plotting $\log L$ against $\log \tau$ and estimating the slope using a least squares linear regression.

$$D = 1 - \lim_{\tau \to 0} \quad \delta \log L / - \delta \log \tau \tag{3}$$

The reliability of the technique was ensured by following the procedures proposed by Klinkenberg (1994). Examples of the use of this technique in geosciences include Goodchild and Mark (1987) and Aviles et al. (1987). Compared to other methods, the divider method is less computationally expensive, easier to use and gives equally good results (Angeles et al., 2004).

3.4. Determining the geometric similarity of headwalls

We based the determination of geometric similarity on the homothetic transformation concept. For each of the one hundred and fifteen headwalls, the following method was used. The extracted headwall was rotated so that its initial and final vertices were aligned horizontally from west to east (Fig. 3a). The curved part of the headwall was always on the top. The mid-point between the initial and final vertex of each headwall was

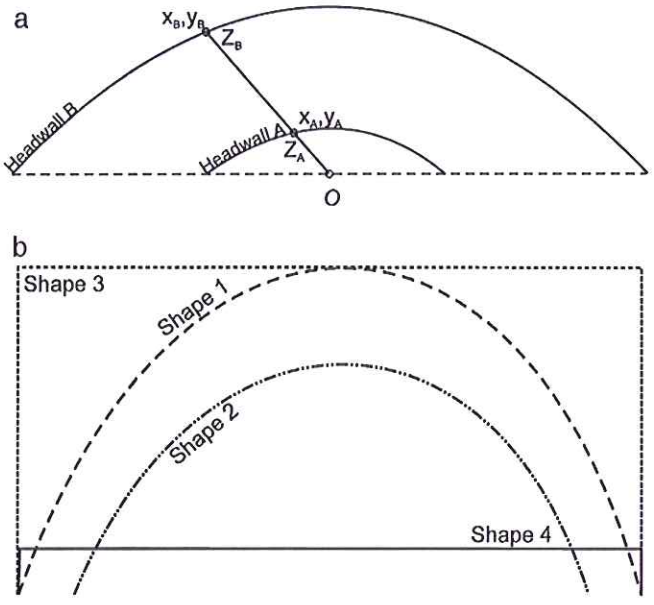

Fig. 3. (a) Illustration of the method used to determine geometric similarity. The distance of point Z_A on headwall A was calculated from O using the x- and y-coordinates. The same was repeated for the corresponding point on headwall B. This was carried out for all the points on the headwalls. The two sequences of data were then compared using linear regression. (b) Shapes used for the sensitivity analysis of the method for the calculation of the similarity coefficient.

determined, and the mid-points for all headwalls were moved to a common position, *O* (Fig. 3a).

For each pair of headwalls, it was first ensured that both headwalls had the same number of co-ordinates. This involved using simple linear interpolation for the shorter headwalls to estimate the position of intermediate points between the extracted co-ordinates. Then, for each headwall, the distance of each co-ordinate from *O* was calculated (in m) (Fig. 3a). The same was repeated for the second headwall. At this point we had two sequences of data. We used regression analysis to understand how similar these sequences were. The distance of each point from the first headwall was plotted against the distance of the corresponding point from the second headwall. A linear trend line starting from the origin was fitted to the plot using least squares linear regression, and the R^2 value was determined. This value represents how similar the sequences of data, and therefore the two headwalls, are (with 1 indicating perfect similarity, and 0 showing no similarity). This value is termed the similarity coefficient. This procedure was carried out for all pairs of headwalls in Storegga (a total of >13 000 pairs).

3.4.1. Sensitivity analysis

The above technique was tested using the basic shapes shown in Fig. 3b. The calculated similarity coefficients for pairs of shapes are shown in Table 1. The highest similarity is observed between shapes 1 and 2, and the lowest between shapes 2 and 4. A visual comparison of the shapes supports the results (Fig. 3b).

4. Results

4.1. Frequency–magnitude relationship

The areas of the individual mass movements identified within the Storegga Slide ranged between 0.27 km^2 and 1972 km^2, with a mean of 42.92 km^2 and a median of 7.19 km^2. These compare to a mean of 233.68 km^2 and a median of 20.75 km^2 for the fifty-eight mass movements identified by Haflidason et al. (2004), which demonstrate the capability of geomorphometric mapping to better identify the small-scale mass movements. To enable comparison with previous studies and model results, the distribution is presented as a linearly binned non-cumulative distribution (Fig. 4). A non-cumulative distribution is defined in terms of the negative of the derivative of the cumulative distribution with respect to *A* (Guzzetti et al., 2002). It is calculated by approximation of the slope of the best-fit line to five adjacent cumulative data points. The result is then normalized to total area. The data in the non-cumulative

Table 1
Geometric similarities for pairs of shapes considered in the sensitivity analysis

	Shape 1	Shape 2	Shape 3	Shape 4
Shape 1	1	0.8895	0.5272	0.0196
Shape 2	0.8895	1	0.4418	0.0110
Shape 3	0.5272	0.4418	1	0.0563
Shape 4	0.0196	0.0110	0.0563	1

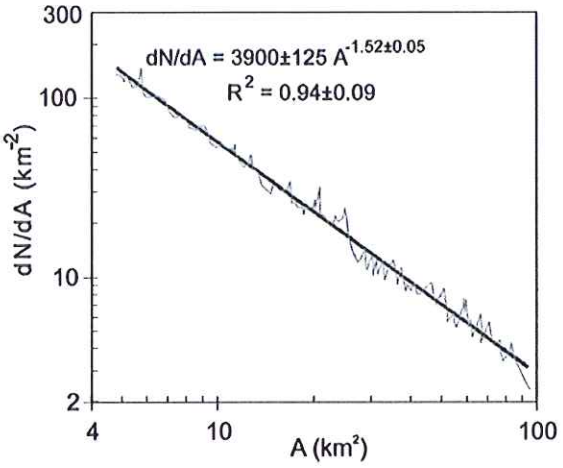

Fig. 4. Non-cumulative frequency-area distribution for the mass movements associated with the one hundred and five individual headwalls extracted in this study.

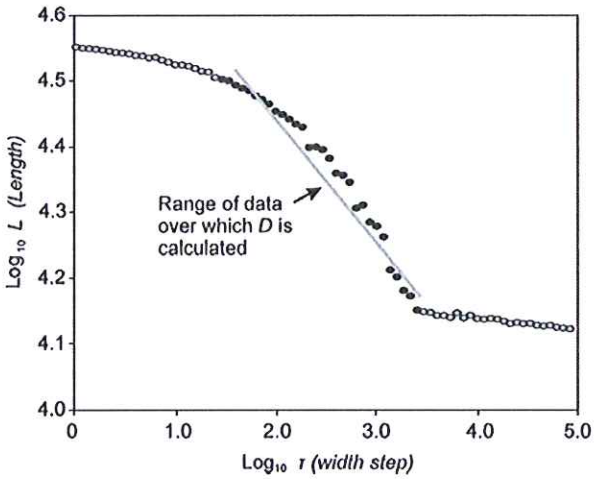

Fig. 5. Richardson plot for a composite headwall (number 67 in table included in supplementary material). The data points shaded in grey indicate the section of the plot where edge effects reduce the fractal dimension *D* of the headwall. The range over which linear regression can be applied, and *D* can be estimated, is indicated by the black data points.

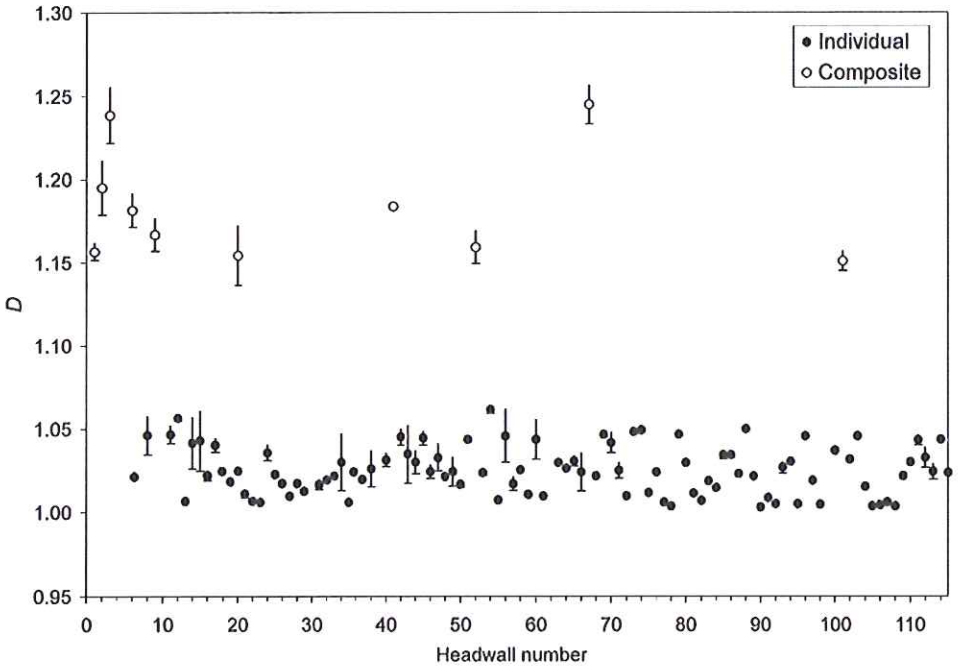

Fig. 6. Plot of the calculated fractal dimension D for all extracted headwalls. The standard deviation for each headwall is also shown.

distribution can be best correlated with a negative power function:

$$dN/A = 3900 \pm 125A^{-1.52\pm0.05} \quad (4)$$

where

N cumulative number of mass movements with an area $>A$

This distribution implies that the low magnitude (small area) mass movements are more frequent than the higher magnitude (large area) mass movements, and that the change in frequency is to the power of 1.52. The range of area over which this relationship is valid is 0.3–100 km^2.

4.2. Fractal analysis

The logs of L and τ (both in m) were plotted for each headwall on a Richardson plot (Fig. 5). For most headwalls, the right hand side of the Richardson plot is characterized by a null slope because the highest magnitudes of τ cannot discriminate the large-scale roughness elements of the headwall trace. This is an edge effect in the measurement that tends to reduce the apparent fractal dimension of the headwalls. The data points on the right hand side of the plot were thus not taken into consideration when calculating the fractal dimension D. Additionally, on the left hand side of the Richardson plot, as τ decreases and approaches the limit of data resolution, L is also asymptotic (Fig. 5). The values influenced by this effect were also excluded from the calculations. A least squares line was fitted to the remaining data (Fig. 5). The R^2 value obtained for each headwall was generally higher than 0.95. To test how well the assumption of linear regression for the data points is satisfied we analyzed the residual structure of the least squares linear regression for each headwall (Andrle, 1992; Klinkenberg and Goodchild, 1992). The standardized residuals were plotted from the best fitting line and the data distribution was analyzed. In all the cases, the distribution of the residuals showed no obvious pattern, the data points were evenly distributed between positive and negative values and they lay between ±2 standard deviations. This shows that the linear regression model is appropriate for our data set. Therefore the gradient of each line of fit was determined from the Richardson plot and the fractal dimension was calculated accordingly.

Table 2
Mean similarity coefficients (and associated standard deviations) for the two identified classes of individual headwalls

	Class 1	Class 2
Class 1	0.7666 (±0.0221)	0.6112 (±0.0895)
Class 2	0.6112 (±0.0895)	0.7399 (±0.0210)

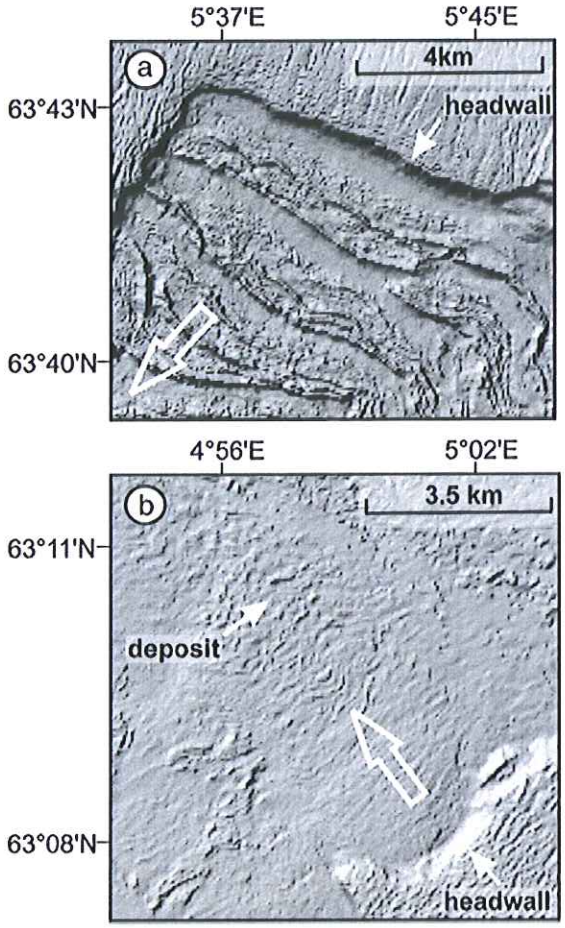

Fig. 7. Shaded relief map of (a) a spread and (b) a debris flow. The headwall formed by the debris flow is more curved compared to that formed by the spread. The large white arrow indicates the direction of mass movement. The locations of the maps are shown in Fig. 1.

The fractal dimensions D of the individual and composite headwalls are shown in Fig. 6. All the values of D are statistically significantly higher than 1, which means that all headwalls have a detectable fractal character. The values of D for the composite headwalls range between 1.15 and 1.25, whereas the values of D for the individual headwalls are close to the Euclidean value of 1. This means that composite headwalls are irregular, whereas individual headwalls are smoother features. Since composite headwalls are comprised of individual headwalls, the scale over which the fractal character is observed in the composite headwalls is not infinite, but it occurs above the lengths of the constituent individual headwalls. The values of D for both individual and composite headwalls do not correlate with size, mass movement type, sediment thickness or depth, which indicates that D is generally homogeneous.

4.3. Geometric similarity

The hundred and five individual headwalls were grouped into two classes according to the mass movement type that formed the headwall: (i) class 1: headwalls formed by spreads; (ii) class 2: headwalls formed by debris flows. The mean similarity coefficients within and between classes are shown in Table 2. The mean similarity coefficients within classes are higher than 0.7. The differences in similarity coefficients between classes are higher than the standard deviation. This means that the differences are statistically significant and that the headwall morphology is determined by the formative mass movement. A visual examination of the headwalls reveals that, in general, headwalls formed by debris flows are more curved than those formed by spreads (Fig. 7). The mean length–width ratio for headwalls in class 1 is 5.64, compared to 3.63 for headwalls in class 2 (where length is measured along a straight line joining the headwall extremities, and the width is the maximum perpendicular distance of the headwall from this line). The headwall lengths in both classes span over almost the entire range of lengths, indicating that spreads and debris flows occur at all scales.

Composite headwalls consist of individual headwalls of varying lengths formed by debris flows or spreads. The ten composite headwalls were arranged into two groups, classes A and B, until the highest intra-group mean similarity coefficients were achieved (Table 3). Within each class, the mean similarity coefficient is very high (>0.8). The difference between the two classes based on geometric similarity is also statistically significant. Fig. 8(a and b) displays an example of a composite headwall from each class. The headwalls in class B, particularly the main slide headwall, can be described as cauliflower-shaped (Canals et al., 2004). The headwalls of numerous submarine landslides around the world may be described in this way, e.g. Gebra Slide (Imbo et al., 2003), Hinlopen Slide (Vanneste et al., 2006), Arecibo Slide (ten Brink et al., 2006b). A comparison of the headwall shapes in Fig. 8 confirms that the shape and length–width ratio of the headwalls of the Gebra,

Table 3
Mean similarity coefficients (and associated standard deviations) for the two identified classes of composite headwalls

	Class A	Class B
Class A [a]	0.8090 (±0.0103)	0.6667(±0.0187)
Class B [b]	0.6667 (±0.0187)	0.8237 (±0.0109)

[a] Class A headwalls: 1, 20, 52, 67, 101 (see supplementary material).
[b] Class B headwalls: 2, 3, 6, 9, 41.

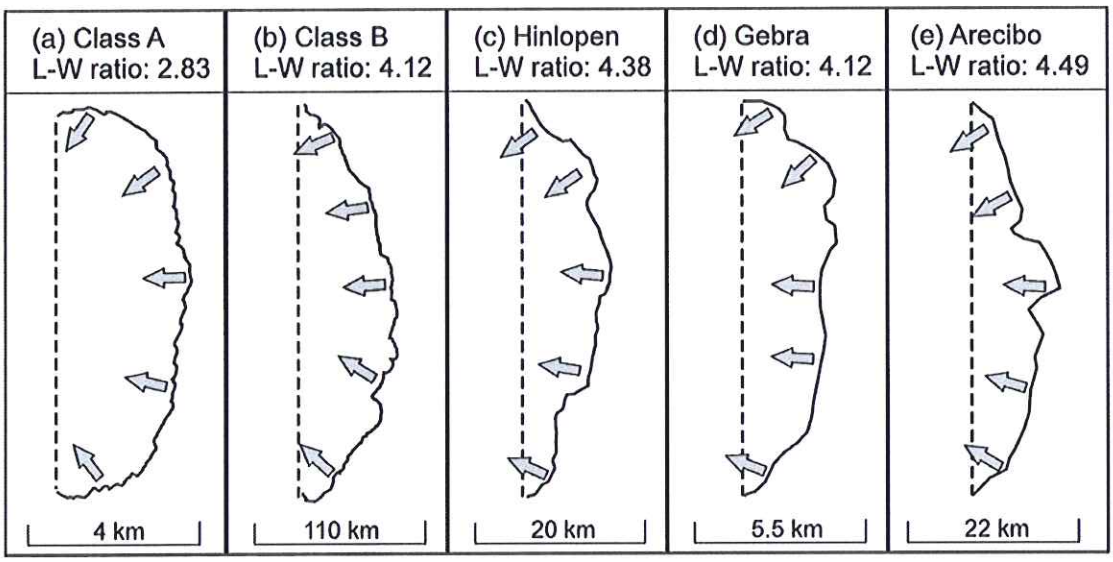

Fig. 8. Comparison of examples of composite headwalls from classes A and B, with the main headwalls of the Hinlopen, Gebra and Arecibo Slides. The headwall in (b) is the Storegga main headwall. The (c) Hinlopen, (d) Gebra and (e) Arecibo slide headwalls were traced from Vanneste et al. (2006), Imbo et al. (2003) and ten Brink et al. (2006b), respectively. The length–width ratio (L–W ratio) refers to the quotient of the length of a straight line joining the headwall extremities, to the maximum perpendicular distance of the headwall from this line. The shape and L–W ratio of the Hinlopen, Gebra and Arecibo Slides are more similar to the class B headwall.

Hinlopen and Arecibo Slides are similar to the composite headwall in class B. The percentage of the total length of composite headwalls formed by debris flows to that formed by spreads is plotted in Fig. 9. This shows that the majority of the headwalls in class A are formed by debris flows, whereas the majority of the headwalls in class B are comprised of spreads. Thus, the shape of the composite headwalls is dependent on the formative mass

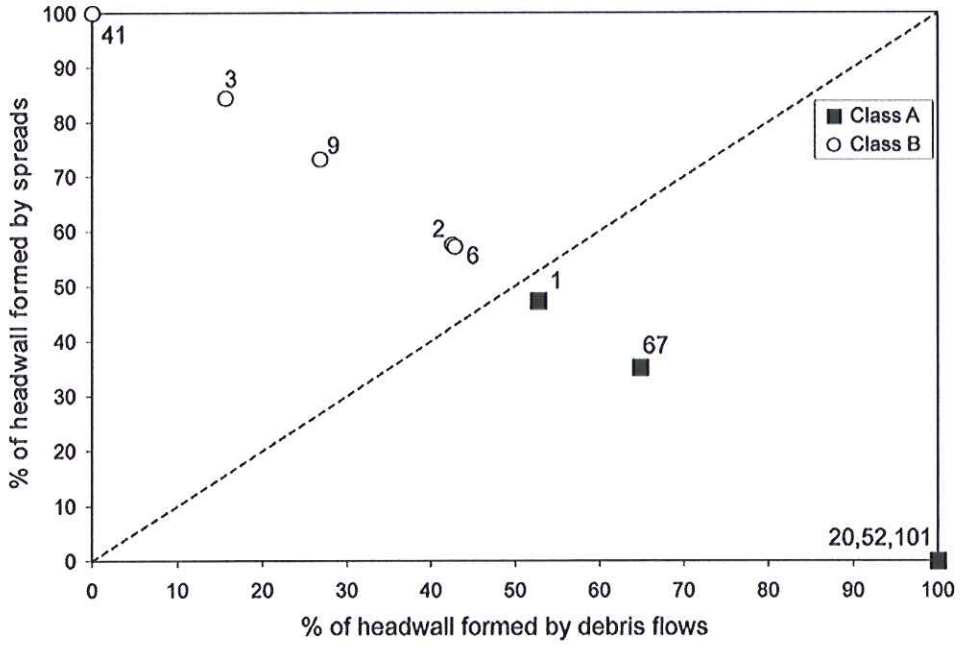

Fig. 9. Plot of the percentage length formed by either spreads or debris flows within each of the ten composite headwalls. The numbers on the graph denote the headwall number (see supplementary material). The composite headwalls have been divided into classes A and B according to the estimated geometric similarity between them. The plot shows that the majority of the length of the composite headwalls in class A is formed by debris flows, whereas the majority of the length of the composite headwalls in class B is formed by spreads.

Table 4
Mean similarity coefficients (and associated standard deviations) between the classes of composite headwalls (A–B) and classes of individual headwalls (1–2)

	Class 1	Class 2
Class A	0.6099±0.0139)	0.7847(±0.0107)
Class B	0.8518±0.0023)	0.6018(±0.0072)

movements. The headwalls of the Hinlopen, Arecibo and Gebra Slides should mainly have been formed by spreads, because the shape and length–width ratio of these landslides is similar to that of the headwalls in class B (Fig. 8). This inference is partly confirmed by the field data. High-resolution swath bathymetry data from the Hinlopen Slide show extensive areas of parallel ridges and troughs close to the main headwall (Figs. 2 and 3 in Vanneste et al., 2006). The resolution of the bathymetric data from the Gebra and Arecibo Slides is not high enough to allow us to identify such ridge and trough morphology (Imbo et al., 2003; ten Brink et al., 2006b). In the case of the Arecibo Slide, however, the failing material consisted of either carbonate layers or oceanic crust. Such material is more likely to fail as a coherent rather than an internally deformable mass (ten Brink et al., 2006b).

The mean similarities between the two classes of composite headwalls and the two classes of individual headwalls are shown in Table 4. Class A headwalls are more similar to class 2 headwalls (formed by debris flows), whereas class B headwalls are more similar to class 1 headwalls (formed by spreads). This indicates that a composite headwall has a similar shape to the majority of the individual headwalls that form it, which implies self-similarity.

5. Discussion

5.1. Scale invariant characteristics of submarine mass movements: origin and significance

The results in Section 4 are evidence of spatial scale invariance within the Storegga Slide. The first type of spatial scale invariance is observed in the distribution of mass movement areas. The frequency of occurrence of submarine mass movements within the Storegga Slide is a function of the mass movement area (or magnitude) according to an inverse power law, and can thus be described as fractal. Similar power law distributions have been identified in numerous inventories of subaerial mass movements of different types and sizes, occurring in a range of environmental settings and triggered by a variety of mechanisms (e.g. Dai and Lee, 2002; Dussauge et al., 2003; Guzzetti et al., 2002; Hovius et al., 1997; Ohmori and Hirano, 1988). A difference between these studies of subaerial landslide populations and our study is that the former have taken into consideration individual landslides whereas we investigated a single, large landslide complex. In this study, the power law scaling of mass movement area with frequency is restricted to the range 0.3–100 km^2. The scaling is observed over ~2.5 orders of magnitude of the area (Fig. 4) (compared to ~3 for data from subaerial mass movements (Hergarten and Neugebauer, 1998)), and can be applied to the majority of the mass movements under consideration.

Explaining the origin of this first type of spatial scale invariance in geological terms is difficult. One explanation is that the fractal distribution is a manifestation of self-organized criticality (SOC) (Bak et al., 1987; Bak et al., 1988), a concept which has found wide application in physics, biology and economics (Bak, 1996). Self-organized criticality is a property of a complex system related to principles of energy dissipation and the occurrence of spatiotemporal chaos (Phillips, 1995). Self-organized criticality may explain the phenomenon whereby, despite complexity and heterogeneity at the level of individual elements (e.g. grains of sediment), the aggregate behavior of the system at the larger scale exhibits order in the form of a fractal distribution. In this complex system, the "input" is nearly constant and the "output" is characterized by a series of events, the frequency-size distribution of which follows a power law in space and time. Emergence of this order occurs through autogenic dynamics and internal feedback mechanisms of the system (Phillips, 1995).

There are a number of necessary conditions for identifying self-organized criticality in a system (Bak et al., 1987): (a) the distribution of event sizes is scale invariant, (b) the system is in a quasi-stationary (critical) state and (c) the temporal behavior of the system is a $1/f$ (red) noise (Bak et al., 1987). Within the Storegga Slide, the distribution of mass movements has been shown to be spatially scale invariant, but we cannot characterize the temporal behavior due to a low temporal resolution of submarine mass movement data. Landsliding is a dissipative phenomenon because material is moved downslope or removed from the slide scar. A continuous, long term driving force is thus required to keep the landslide in a quasi-stationary state. In the Storegga region, this force is represented by the continuous and variable deposition of glacially-derived material (during glacial maxima) and hemipelagic sedimentation (during interglacials) that has been taking place along the mid-

Norwegian Margin during at least the last 3 Ma (Rise et al., 2005). These processes have resulted in a progressive increase in sediment pore pressure, gravitationally-induced stress and surface slope gradient, all of which promote slope instability. Another driving force may comprise seismic activity, because glacially-induced tectonic movements enable the Storegga Slide system to exceed thresholds and trigger slope instabilities (Evans et al., 2005). Such conditions are all typical of a system in a critical state. In consideration of the above, we conclude that the Storegga Slide is a geomorphological system that may exhibit self-organized criticality.

One of the most widespread models of self-organized criticality is the Bak–Tang–Wiesenfeld (BTW) model (Bak et al., 1988), also known as the 'sandpile' model. This simple cellular automata model consists of a lattice where particles are dropped into a randomly selected grid at time steps. When the total number of particles in a grid exceeds a specific threshold, the site collapses and the particles are redistributed into the adjacent grids. The redistribution of particles can lead to an 'avalanche'. Numerical studies have shown that, in a 'sandpile' model, the non-cumulative number of 'avalanches' with the 'avalanche' area satisfies a power law distribution, and that the value of the exponent of the power law is ~ 1 (Kadanoff et al., 1989). The exponent associated with the spatial power law scaling of subaerial mass movements is significantly higher than 1. The values range between 2.2 and 3.3 for mass movements occurring in a variety of environmental settings (Dai and Lee, 2002; Guzzetti et al., 2002; Hovius et al., 1997; Malamud et al., 2004; Van Den Eeckhaut et al., 2007). The value of the exponent obtained for submarine mass movements within the Storegga Slide is 1.52. This value is still higher than the 'sandpile' model value of 1. This difference can be attributed to the simplicity of the 2D 'sandpile' model, which contrasts with the multitude of forces and controls operating on a variety of spatiotemporal scales in 3D in mass movements. For example, a higher exponent of landslide frequency-size distribution has been obtained when incorporating factors such as geological heterogeneity (Sugai et al., 1994), soil moisture content (Pelletier et al., 1997) and slope stability considerations (Hergarten and Neugebauer, 1998) into landslide models. On the other hand, the value of the exponent for submarine mass movements is considerably lower than for subaerial mass movements, and closer to the 'sandpile' model value. This could imply that, in comparison to subaerial mass movements, submarine mass movement systems are less complex and that their dynamics are more analogous to those of the 'sandpile' model. The elements in the 'sandpile' model can be qualitatively related to the components of the Storegga Slide system. The dropping particles represent sediment deposition, the avalanches are the individual mass movements, and the thresholds are associated with changes in slope gradient, pore pressure and gravitationally-induced stress. In subaerial systems, on the other hand, driving forces such as tectonic uplift and fluvial incision tend to interact with weathering forces, variable degrees of saturation, high geological heterogeneity and topographic roughness, yielding a higher exponent for the power law distribution of mass movements. Since the sediments failing within the Storegga Slide are mainly clays, cohesive forces may be another factor explaining the low exponent associated with submarine mass movements. Since the exponent for the Storegga mass movements' distribution is <2 and lower than the values obtained for subaerial mass movements, we can also infer that the larger mass movements are more dominant in submarine environments.

The applicability of the 'sandpile' model to submarine mass movements is not without problems, however. First, aspects of inertia and cohesion are overlooked in the 'sandpile' model. Secondly, self-organized criticality is not a property unique to cellular automata models. Hergarten and Neugebauer (1998), for example, developed a model of landsliding that exhibits self-organized criticality using partial differential equations only. For our study area, another explanation of the fractal distribution of the mass movements is the fact that the Storegga Slide was a retrogressive slope failure (Haflidason et al., 2005; Kvalstad et al., 2005). Instability did not occur across the entire slip surface simultaneously, but started as one or a few large mass movements located close to the Faroe–Shetland Escarpment (Haflidason et al., 2004). Failure in this region destabilized the neighboring areas and the instability propagated upslope via the progressive collapse of the headwall. The area of the mass movements within the Storegga Slide become smaller with distance upslope (Haflidason et al., 2004; Issler et al., 2005), whilst the number of mass movements increases (Fig. 10). Therefore, as the slope failure propagated upslope, each mass movement triggered an increasing number of smaller mass movements, in the style of a cascade. The continental slope is characterized by extensive areas of uniform gentle topography (Shepard, 1963). In such a setting the boundary conditions are largely homogeneous and a retrogressive cascade would be allowed to develop unobstructed. The Storegga retrogressive cascade continued until the boundary conditions changed at the limits of the present Storegga Slide scar. These changes include the decrease in the slope gradient of the seabed where the continental slope meets the continental shelf, and the

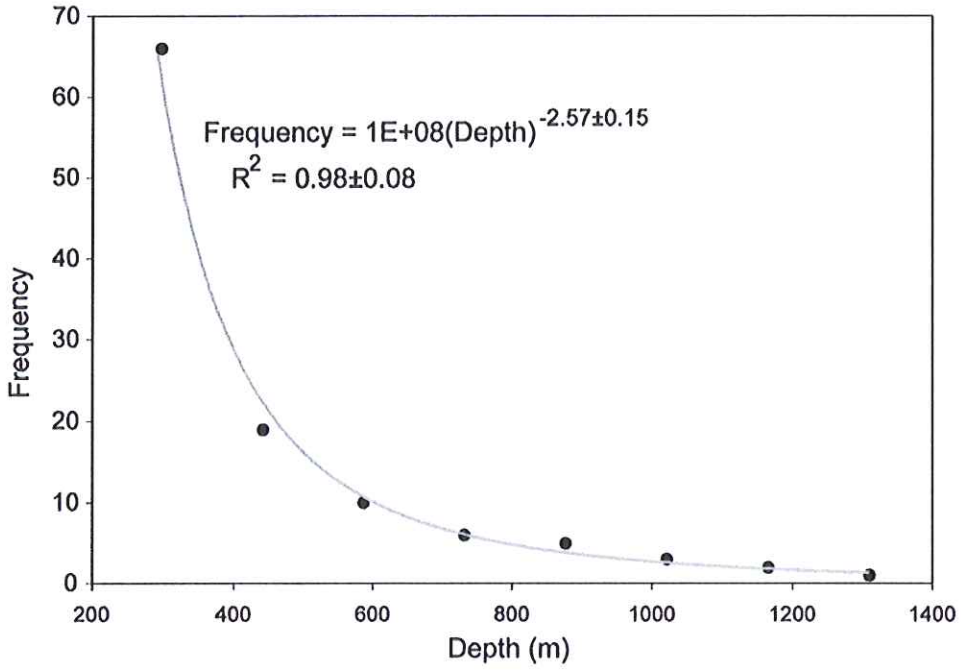

Fig. 10. Frequency-depth distribution of the one hundred and five individual headwalls.

gradation into pronounced morphological barriers (the North Sea Fan in the south and the Vøring Plateau in the north). Another factor responsible for halting the retrogressive cascade must have been the increase in the consolidation of the sediments in the region of the Storegga Slide main headwall, due to glacial compaction during the Last Glacial Maximum (Gauer et al., 2005). The Storegga retrogressive cascade is qualitatively similar to the activation of avalanches in the 'sandpile' model and may explain the power law of the frequency-area distribution of the submarine mass movements.

Self-organized criticality is, however, not the only explanation of the observed spatial power law scaling in submarine mass movements. Pre-defined geological structures and natural variability may also result in a spatial power law distribution in mass movements, without the need of self-organized criticality (Hergarten, 2003; Pelletier et al., 1997). Detailed information about the spatial variability of geotechnical properties and geological structures within the Storegga Slide is not available. Thus we are unable to confirm a potential relationship between the power law distribution of mass movements and geological structures.

A second type of spatial scale invariance within the Storegga Slide is identified in mass movement morphology. The plot of headwall length vs. mass movement area in Fig. 2 shows strong power law scaling. The geometric similarity of headwalls at different scales (Table 2) and the self-similar properties of the composite headwalls (Table 4; Fig. 6) are also indicative of morphological scale invariance. These results complement the observations made by Issler et al. (2005) for mass movements within the Storegga Slide, where the area of a longitudinal section across the mass movements was found to scale with the released volume. The geometric scaling behavior of landslides implies that the form and the geological processes associated with submarine mass movements are the same at the investigated scales. In the absence of other factors, such as heterogeneities in the failing material, this observation indicates that the inclusion of hydroplaning and shear wetting in physical models of slope failures by Issler et al. (2005) can be extended to the different scales investigated in this study.

5.2. Headwalls as morphological proxies

The two classes of composite headwalls are geometrically similar to the majority of their constituent headwalls. This observation, combined with the high values of the fractal dimension D observed in composite headwalls, indicates that the composite headwalls formed by submarine mass movements are self-similar at scales higher than those of the constituent individual headwalls. This means that when headwalls from separate mass movements coalesce, the resulting headwall has a shape similar to its constituent headwalls, or to those which occupy the largest portion of the headwall (if formed by

different types of mass movement). The shape of individual headwalls was shown to be indicative of its principal formative geological processes. This also applies to composite headwalls. Headwalls formed by spreads have a length–width ratio higher than ~4 and their shape ranges between cauliflower-shaped and linear. Headwalls formed by debris flows are more curvilinear and have a length–width ratio lower than ~4. This observation provides a basis for a morphological classification of submarine landslides and allows the identification of mass movement type even when the resolution of the bathymetric data is low and only the shape of the headwall is discernible. The difference in shape may be explained by the fact that a higher level of plastic deformation is required to evacuate a curvilinear headwall, in comparison to a quasi-linear headwall, where deformation entails brittle deformation of the sediment into coherent blocks. The reasons for why some slope failures form spreads, whereas other transform into debris flows, may be various. Subtle differences in the physical properties of the sediment could influence the type of deformation. Boundary effects, presence of gas hydrates, variation in sediment facies (e.g. presence of contourites), and evolution of the landslide, may also be important. The fractal dimension of headwalls, on the other hand, can be used to reveal whether a headwall is formed by one or more mass movements. Thus, headwalls can be used as morphological proxies for the identification of submarine mass movements.

5.3. Implications

There are several important implications that result from the study of the fractal statistics and morphology of the Storegga Slide. The first relates to the design of systems to investigate and model submarine mass movements. Self-organized criticality is advocated as the most likely explanation of the observed power law in the frequency-area distribution of submarine mass movements within the Storegga Slide. The Storegga Slide may thus be modelled as a large-scale geomorphic system in a quasi-stationary state, and power law relations may be incorporated in the evolution modelling of this landslide. Submarine mass movements are more comparable to the theoretical 'sandpile' model than their subaerial counterparts, and should therefore be simpler to model. Self-organized criticality is an emergent property that is not built into the physical equations a priori (Gupta, 2004). The aggregate behavior of a large-scale geomorphic system such as the Storegga Slide may therefore be independent of the smaller-scale components. Not all aspects of the submarine mass movement system can be reproduced by modeling the small-scale elements of the system, as espoused by the engineering approach. This also means, however, that limitations in data acquisition techniques that do not have the adequate resolution can be circumvented when considering emergent features. The spatial scale invariant behavior of mass movement morphology within the Storegga Slide contradicts the long-standing geographic tradition that geomorphic processes operate at specific spatial scales (Schumm and Lichty, 1965). If mass movements are scale invariant, then the morphology and mechanisms of mass movements can be extrapolated from the small-scale to the large-scale (or vice versa). The retrogressive cascade, based on loss of support as the threshold exceeding mechanism in this open system, also explains the power law distribution of mass movements. It fits the self-organized critical behavior well and emphasises the importance of considering the interconnectivity of individual landslides. The evolution of a retrogressive cascade on a continental slope, where boundary conditions are generally homogeneous, would explain the large size of the Storegga Slide and similar submarine landslides elsewhere.

The second important implication is that our results also provide an explanation for the potential similarity in the shape of headwalls of submarine mass movements around the world. Spreading is a retrogressive mass movement (Kvalstad et al., 2005; Micallef et al., 2007). Ridge and trough morphology, characteristic of spreading, can be observed in numerous submarine landslides around the world. In this study we observed that the cauliflower-shape of the Storegga Slide headwall is mainly associated with spreading, and that this shape is also common in submarine mass movements, particularly in formerly glaciated margins such as the Norwegian Margin. Analysis of landslides in the North Atlantic shows that mass movements mainly initiate in the mid-continental slope (Hühnerbach and Masson, 2004), and that they develop progressively upslope (Kvalstad et al., 2005). If we combine these observations we can propose that the majority of submarine mass movements develop retrogressively, with spreading as the latest stage of the slide evolution that defines the main headwall. Since spreading can be linked with the retrogressive cascade, self-organized critical behavior could potentially be an emergent feature of numerous submarine mass movements throughout the world.

The third implication relates to mass movements as natural geohazards. Frequency-magnitude plots of mass movements can be re-cast as probability distributions, providing a measure of the hazard risk posed by such slope failures (Guzzetti et al., 2002). By plotting the frequency–magnitude distribution of the mass movements we can estimate the event magnitude, along with

the total number and volume of mass movements, and extrapolate incomplete inventories within the limits of power law behavior (in the case of the Storegga Slide, for mass movements ranging between 0.3–100 km^2 in area). These considerations are particularly useful in tsunami hazard assessment, where knowledge of probabilities of the causative mass movement size is required (ten Brink et al., 2006a). Within the Storegga Slide, the larger mass movements are more dominant than in subaerial settings. This means that it is sufficient to obtain an accurate inventory of the larger mass movements in order to understand the frequency–magnitude characteristics of all the mass movements that comprise the Storegga Slide. In our acoustic data sets, as in those of other submarine landslides, the larger mass movements are generally well-resolved.

6. Conclusions

In this study we presented evidence of the scale invariant characteristics of the Storegga Slide. The frequency-area distribution of mass movements within the Storegga Slide satisfies an inverse power law. Headwalls are geometrically similar at a wide range of scales, and headwall lengths scale with mass movement areas. Composite headwalls are self-similar features. These characteristics of the Storegga Slide provide an important insight into the physics of submarine slope failure, and support the concepts of scale invariance and self-organized criticality in submarine slide evolution theory and modeling. The origin of spatial scale invariance may also be associated to the retrogressive nature of the Storegga Slide. Our results are important in terms of the morphological classification of submarine mass movements, because headwall shape can be used as a morphological proxy for the formative mass movements.

Acknowledgements

This research was supported by the HERMES project, EC contract no. GOCE-CT-2005-511234, funded by the European Commission's Sixth Framework Programme under the priority 'Sustainable Development, Global Change and Ecosystems'. We would like to thank Norsk Hydro ASA for providing the bathymetric data and 2D seismic lines. BP Norway and the European North Atlantic Margin (ENAM) II Programme are acknowledged for making available the 3D seismic dataset and TOBI sidescan sonar imagery, respectively. We are grateful to Dr. Robin S. Snow for sharing the FORTRAN code for the divider method. The insightful comments of two anonymous reviewers are greatly appreciated.

Appendix A. Supplementary data

Supplementary data associated with this article can be found, in the online version, at doi:10.1016/j.margeo.2007.08.003.

References

Andrle, R., 1992. Estimating fractal dimension with the divider method in geomorphology. Geomorphology 5 (1–2), 131–141.

Angeles, G.R., Perillo, G.M.E., Piccolo, M.C., Pierini, J.O., 2004. Fractal analysis of tidal channels in the Bahía Blanca Estuary (Argentina). Geomorphology 57, 263–274.

Aviles, C.A., Scholz, C.H., Boatwright, J., 1987. Fractal analysis applied to characteristic segments of the San Andrea Fault. J. Geophys. Res. 92 (B1), 331–344.

Bak, P., 1996. How nature works: the science of self-organized criticality. Copernicus. Springer, New York.

Bak, P., Tang, C., Wiesenfield, K., 1987. Self-organized criticality: an explanation of 1/*f* noise. Phys. Rev. Lett. 59, 381–384.

Bak, P., Tang, C., Wiesenfield, K., 1988. Self-organized criticality. Phys. Rev., A. 38, 364–374.

Berg, K., Solheim, A., Bryn, P., 2005. The Pleistocene to recent geological development of the Ormen Lange area. Mar. Pet. Geol. 22 (1–2), 45–56.

Canals, M., Lastras, G., Urgeles, R., Casamor, J.L., Mienert, J., Cattaneo, A., De Batist, M., Haflidason, H., Imbo, Y., Laberg, J.S., Locat, J., Long, D., Longva, O., Masson, D.G., Sultan, N., Trincardi, F., Bryn, P., 2004. Slope failure dynamics and impacts from seafloor and shallow sub-seafloor geophysical data: case studies from the COSTA project. Mar. Geol. 213 (1–4), 9–72.

Dai, F.C., Lee, C.F., 2002. Landslide characteristics and slope instability modeling using GIS, Lantau Island, Hong Kong. Geomorphology 42, 213–228.

Dussauge, C., Grasso, J.R., Helmstetter, A., 2003. Statistical analysis of rockfall volume distributions: implications for rockfall dynamics. J. Geophys. Res. 108 (B6), 2286.

Evans, D., Harrison, Z., Shannon, P.M., Laberg, J.S., Nielsen, T., Ayers, S., Holmes, R., Hoult, R.J., Lindberg, B., Haflidason, H., Long, D., Kuijpers, A., Andersen, E.S., Bryn, P., 2005. Palaeoslides and other mass failures of Pliocene to Pleistocene age along the glaciated European margin. Mar. Pet. Geol. 22 (9–10), 1131–1148.

Gauer, P., Kvalstad, T.J., Forsberg, C.F., Bryn, P., Berg, K., 2005. The last phase of the Storegga Slide: simulation of retrogressive slide dynamics and comparison with slide-scar morphology. Mar. Pet. Geol. 22 (1–2), 171–178.

Goodchild, M.F., Mark, D.M., 1987. The fractal nature of geographic phenomena. Ann. Assoc. Am. Geogr. 77, 265–278.

Gupta, V.K., 2004. Emergence of statistical scaling in floods on channel networks from complex runoff dynamics. Chaos, Solitons Fractals. 19, 357–365.

Guzzetti, F., Malamud, B.D., Turcotte, D.L., Reichenbach, P., 2002. Power-law correlations of landslide areas in central Italy. Earth Planet. Sci. Lett. 195, 169–183.

Guzzetti, F., Reichenbach, P., Cardinali, M., Galli, M., Ardizzone, F., 2005. Probabilistic landslide hazard assessment at the basin scale. Geomorphology 72, 272–299.

Haflidason, H., Sejrup, H.P., Nygård, A., Bryn, P., Lien, R., Forsberg, C.F., Berg, K., Masson, D.G., 2004. The Storegga Slide: architecture, geometry and slide-development. Mar. Geol. 231, 201–234.

Haflidason, H., Lien, R., Sejrup, H.P., Forsberg, C.F., Bryn, P., 2005. The dating and morphometry of the Storegga Slide. Mar. Pet. Geol. 22 (1–2), 123–136.

Hergarten, S., 2003. Landslides, sandpiles and self-organised criticality. Nat. Hazards Earth Syst. Sci. 3, 505–514.

Hergarten, S., Neugebauer, H.J., 1998. Self-organized criticality in a landslide model. Geophys. Res. Lett. 25 (6), 801–804.

Hovius, N., Stark, C.P., Allen, P.A., 1997. Sediment flux from a mountain belt derived by landslide mapping. Geology 25 (3), 231–234.

Hühnerbach, V., Masson, D.G., 2004. Landslides in the North Atlantic and its adjacent seas: an analysis of their morphology, setting and behaviour. Mar. Geol. 213, 343–362.

Imbo, Y., De Batist, M., Canals, M., Prieto, M.J., Baraza, J., 2003. The Gebra Slide: a submarine slide on the Trinity Peninsula Margin, Antarctica. Mar. Geol. 193, 235–252.

Issler, D., De Blasio, F.V., Elverhøi, A., Bryn, P., Lien, R., 2005. Scaling behaviour of clay-rich submarine debris flows. Mar. Pet. Geol. 22 (1–2), 187–194.

Kadanoff, L.P., Nagel, S.R., Wu, L., Zhou, S.M., 1989. Scaling and universality in avalanches. Phys. Rev., A. 39, 6524–6533.

Klinkenberg, B., 1992. Fractals and morphometric measures: is there a relationship? Geomorphology 5, 5–20.

Klinkenberg, B., 1994. A review of methods used to delineate the fractal dimensions of linear features. Math. Geol. 26 (1), 23–46.

Klinkenberg, B., Goodchild, M.F., 1992. The fractal properties of topography: a comparison of methods. Earth Surf. Process. Landf. 17, 217–234.

Kvalstad, T.J., Andersen, L., Forsberg, C.F., Berg, K., Bryn, P., Wangen, M., 2005. The Storegga slide: evaluation of triggering sources and slide mechanisms. Mar. Pet. Geol. 22 (1–2), 245–256.

Malamud, B.D., Turcotte, D.L., Guzzetti, F., Reichenbach, P., 2004. Landslides inventories and their statistical properties. Earth Surf. Process. Landf. 29, 687–711.

Mandelbrot, B., 1977. Fractals: Form, Chance and Dimension. WH Freeman, San Francisco.

Mandelbrot, B.B., 1983. The Fractal Geometry of Nature. W.H. Freeman, New York.

Masson, D.G., Harbitz, C.B., Wynn, R.B., Pedersen, G., Løvholt, F., 2006. Submarine landslides: processes, triggers and hazard prediction. Philos. Trans.-R. Soc. 364 (1845), 2009–2039.

Micallef, A., Berndt, C., Masson, D.G., Stow, D.A.V., 2007. A technique for the morphological characterization of submarine landscapes as exemplified by debris flows of the Storegga Slide. J. Geophys. Res. 112, F02001.

Micallef, A., Masson, D.G., Berndt, C., Stow, D.A.V., 2007. The morphology and mechanics of submarine spreading: a case study from the Storegga Slide. J. Geophys. Res. 112, F03023.

Ohmori, H., Hirano, M., 1988. Magnitude, frequency and geomorphological significance of rocky mud flows, landcreep and the collapse of steep slopes. Z. Geomorphol. (Suppl. Bd.). 67, 55–65.

Pelletier, J.D., 1999. Self-organization and scaling relationships of evolving river networks. J. Geophys. Res. 104 (B4), 7359–7375.

Pelletier, J.D., Malamud, B.D., Blodgett, T., Turcotte, D.L., 1997. Scale-invariance of soil moisture variability and its implications for the frequency-size distribution of landslides. Eng. Geol. 48, 255–268.

Phillips, J.D., 1995. Self-organization and landscape evolution. Prog. Phys. Geogr. 19, 309–321.

Rise, L., Ottensen, D., Berg, K., Lundin, E., 2005. Large-scale development of the mid-Norwegian Margin during the last 3 million years. Mar. Pet. Geol. 22 (1–2), 33–44.

Schumm, S.A., Lichty, R.W., 1965. Time, space and causality in geomorphology. Am. Journal Sci. 263, 110–119.

Shepard, F.P., 1963. Submarine Geology, 2nd edition. Harper and Row, London.

Solheim, A., Berg, K., Forsberg, C.F., Bryn, P., 2005. The Storegga Slide complex: repetitive large scale sliding with similar cause and development. Mar. Pet. Geol. 22 (1–2), 97–107.

Southgate, H.N., Möller, N.K., 2000. Fractal properties of coastal profile evolution at Duck, North Carolina. J. Geophys. Res. 105 (C5), 11489–11507.

Steinhaus, H., 1960. Mathematical Snapshots. Oxford University Press, London.

Sugai, T., Ohmori, H., Hirano, M., 1994. Rock control on magnitude–frequency distribution of landslides. Transactions Jpn. Geomorphol. Union. 15 (3), 233–251.

Sultan, N., Cochonat, P., Canals, M., Cattaneo, A., Dennielou, B., Haflidason, H., Laberg, J.S., Long, D., Mienert, J., Trincardi, F., Urgeles, R., Vorren, T.O., Wilson, C., 2004. Triggering mechanisms of slope instability processes and sediment failures on continental margins: a geotechnical approach. Mar. Geol. 213 (1–4), 291–321.

Summerfield, M., 1991. Global Geomorphology: An Introduction to the Study of Landforms. Longman, London.

ten Brink, U.S., Geist, E.L., Andrews, B.D., 2006a. Size distribution of submarine landslides and its implication to tsunami hazard in Puerto Rico. Geophys. Res. Lett. 33, L11307–L11311.

ten Brink, U.S., Geist, E.L., Lynett, P., Andrews, B., 2006b. Submarine slides north of Puerto Rico and their tsunami potential. In: Mercado, A., Liu, P.L.F. (Eds.), Caribbean Tsunami Hazard, World Sci.

Turcotte, D.L., Malamud, B.D., Guzzetti, F., Reichenbach, P., 2006. Self-organization, the cascade model and natural hazards. Proc. Natl. Acad. Sci. U. S. Am. 99 (1), 2530–2537.

Van Den Eeckhaut, M., Poesen, J., Govers, G., Verstraeten, G., Demoulin, A., 2007. Characteristics of the size distribution of recent and historical landslides in a populated hilly region. Earth Planet. Sci. Lett., 256 (3–4), 588–603.

Vanneste, M., Mienert, J., Bünz, S., 2006. The Hinlopen Slide: a giant, submarine slope failure on the northern Svalbard Margin, Arctic Ocean. Earth Planet. Sci. Lett. 245 (1–2), 373–388.

Wolman, M.G., Miller, J.P., 1960. Magnitude and frequency of forces in geomorphic processes. J. Geol. 68, 54–74.